INTERNATIONAL JOURNAL FOR INNOVATIVE RESEARCH IN MULTIDISCIPLINARY FIELD
ISSN(O): 2455-0620 [Impact Factor: 9.47]
Monthly, Peer-Reviewed, Refereed, Indexed Journal with IC Value : 86.87
Volume - 11, Issue - 07, July - 2025

DOIs:10.2015/IJIRMF/202507036 --:-- Research Paper / Article / Review

Dysprosium-Doped Lithium Borate Glasses: Luminescence Behaviour and Suitability for Yellow Lasers

Dr. K. Sudhakar Reddy,
Lecturer in Physics,
General Section, ESC Government Polytechnic, Nandyal, Andhrapradesh, India-518501
Email – [1]sudhakar567@gmail.com

Abstract: ***Dy^{3+}-doped lithium borate (LB) glasses with compositions (in mol%) (55−x) B_2O_3 + 25LiF + 10MgF_2 + 10ZnO + xDy_2O_3 (where x = 0.1, 0.5, 1.0, 1.5, and 2.0 mol%) were synthesized via the melt-quenching technique and systematically investigated through structural, optical, and luminescence studies, including Judd–Ofelt (J–O) analysis.*** *The glass structure was characterized using X-ray diffraction (XRD) and Raman spectroscopy. Optical absorption, photoluminescence, and decay kinetics measurements were performed to analyze the optical properties. From the absorption spectra, oscillator strengths (f) and Judd–Ofelt intensity parameters (Ω_2, Ω_4, Ω_6) were derived. Photoluminescence data, in conjunction with J–O parameters, were used to calculate radiative transition probabilities (A_r), experimental branching ratios (β_{exp}), stimulated emission cross-sections (σ_e), and optical gain ($\sigma_e \times \tau_{exp}$).Lifetimes ($\tau_{exp}$) of the $^4F_{9/2}$ excited level were estimated from decay profiles to evaluate luminescence efficiency across all Dy^{3+} concentrations. The results were compared with existing literature, highlighting the potential of these glasses for yellow laser applications.*

Key Words: *Dy^{3+}-doped lithium borate (LB) glasses, luminescence studies, yellow laser applications.*

1. INTRODUCTION:

In recent years, luminescent materials doped with rare-earth ions have garnered significant attention due to their promising applications in lasers, display technologies, light-emitting diodes (LEDs), and related optoelectronic devices. Rare-earth ions are particularly attractive to researchers owing to their distinctive properties, including low toxicity, excellent photostability, high thermal and chemical stability, and sharp, well-defined emission bands. Among the key parameters influencing the performance of optical devices, luminescence intensity plays a crucial role [1]. This intensity can often be enhanced by increasing the doping concentration of rare-earth ions in a suitable host matrix. Despite considerable progress in developing rare-earth-doped materials using a variety of host systems, continued research is essential to discover more efficient and practical materials for advanced optical devices. One such promising host is **borate glass**, which stands out due to its high thermal and chemical stability, wide transmission window from the ultraviolet (UV) to infrared (IR) region, low refractive index, and high emission cross-sections [2]. These favorable properties are largely attributed to the local structure of boron atoms, whose coordination geometry is influenced by the glass composition and the type of modifiers incorporated into the glass network.

To facilitate higher rare-earth ion solubility, glass modifiers are added to disrupt bridging oxygen bonds and increase non-bridging oxygens. Alkali and alkaline-earth metal oxides typically serve this role, creating environments favorable for rare-earth ion incorporation near non-bridging oxygen sites. However, one of the main drawbacks of oxide-based glasses is their high phonon energy, which can result in non-radiative relaxation and reduced luminescence efficiency. To mitigate this, fluorine is introduced into the glass matrix—often in the form of metal fluorides—resulting in **fluoro-borate glasses**, which combine the beneficial properties of both fluoride and borate systems [3].

Among the various rare-earth ions, **dysprosium (Dy^{3+})** has been extensively studied due to its potential in sensing, laser amplification, and white-light emission applications. Dy^{3+} is particularly useful for white-light generation because its emission spectrum includes blue and yellow bands that correspond to primary visible colors [4].

Understanding the influence of both host composition and dopant concentration is essential for tailoring optical properties to suit practical applications. The present work investigates the spectroscopic properties of a series of Dy^{3+}-doped lithium borate (LB) glasses with fixed base composition and varying Dy^{3+} concentrations. Structural, optical absorption, photoluminescence (PL), and decay kinetics analyses were conducted to characterize these materials.

Furthermore, **Judd–Ofelt (J–O) analysis** was employed to estimate radiative transition probabilities (A_r), branching ratios (β), stimulated emission cross-sections (σ_e), and optical gain ($\sigma_e \times \tau_{exp}$), providing insights into the materials' potential for laser applications.

Recent studies underscore the relevance of Dy^{3+}-doped glasses in luminescent applications. For instance, Hashim et al. [5] examined Dy^{3+}-doped lithium borate glasses as solid-state thermoluminescent (TL) detectors and reported enhanced blue photoluminescence up to 0.5 mol% Dy^{3+}, with quenching at higher concentrations. Meza-Rocha et al. [6] achieved white-light emission using zinc phosphate glasses doped with Eu^{3+} and Dy^{3+}, where Dy^{3+} effectively sensitized Eu^{3+} via non-radiative energy transfer. Similarly, Mhareb et al. [7] explored the effects of Dy_2O_3 doping on the physical, optical, and TL properties of lithium borate glasses. In light of these findings, the present study aims to identify and characterize Dy^{3+}-doped lithium borate glass compositions with enhanced luminescent and radiative properties suitable for yellow laser applications.

2. EXPERIMENTAL:

A series of dysprosium-doped lithium borate (LB) glasses with varying Dy^{3+} concentrations (0.1, 0.5, 1.0, 1.5, and 2.0 mol%) were synthesized using the conventional **melt-quenching technique**. The following high-purity precursor chemicals (99.9%, Himedia) were used: boric acid (B_2O_3), lithium fluoride (LiF), magnesium fluoride (MgF_2), zinc oxide (ZnO), and dysprosium oxide (Dy_2O_3). The glass compositions prepared are listed below:

- **LBDy01**: $59.9B_2O_3 + 20LiF + 10MgF_2 + 10ZnO + 0.1Dy_2O_3$
- **LBDy05**: $59.5B_2O_3 + 20LiF + 10MgF_2 + 10ZnO + 0.5Dy_2O_3$
- **LBDy10**: $59.0B_2O_3 + 20LiF + 10MgF_2 + 10ZnO + 1.0Dy_2O_3$
- **LBDy15**: $58.5B_2O_3 + 20LiF + 10MgF_2 + 10ZnO + 1.5Dy_2O_3$
- **LBDy20**: $58.0B_2O_3 + 20LiF + 10MgF_2 + 10ZnO + 2.0Dy_2O_3$

The precursor powders were weighed in stoichiometric proportions and thoroughly ground in an agate mortar to ensure homogeneity. The resulting mixture was transferred to a porcelain crucible and melted in an electric furnace at **1100 °C for 1 hour**. The molten glass was then rapidly poured onto a preheated brass plate to form bulk glass samples, which were immediately annealed at **250 °C** to relieve internal thermal stresses.

Refractive index (n) measurements were carried out using an **Abbe refractometer** at the sodium D-line wavelength (583.3 nm), using **one-bromonaphthalene** as the contact liquid. **Glass density (d)** was determined via the **Archimedes principle**, using water as the immersion medium.

Structural characterization of the glasses was performed using **X-ray diffraction (XRD)** with a SEIFERT diffractometer to confirm the amorphous nature of the samples. The **Raman spectra** were recorded to identify vibrational modes and structural units in the host glass matrix.

The **optical properties** were studied through absorption, excitation, emission, and decay measurements. Absorption spectra were recorded using a **UV–VIS–NIR spectrophotometer (ELICO SL 218)**. Photoluminescence excitation and emission spectra, along with fluorescence decay profiles, were measured using a **JOBIN YVON Fluorolog-3 spectrofluorometer** equipped with a **xenon lamp** as the excitation source. All optical measurements were carried out at **room temperature**.

3. RESULTS AND DISCUSSIONS

X-RAY DIFFRACTOGRAM (XRD)

The XRD diffractogram of the lithium borate host glass system is shown in Fig. 1. The XRD spectrum clearly confirms the **amorphous nature** of the synthesized glass. A broad, diffuse hump is observed in the range of **$20° < 2\theta < 30°$**, with no sharp or well-defined crystalline peaks, indicating the absence of long-range order. This characteristic halo is typical of glassy materials, confirming that the lithium borate samples possess a **non-crystalline (glassy) phase**. The absence of crystallinity is essential for ensuring uniform optical pro

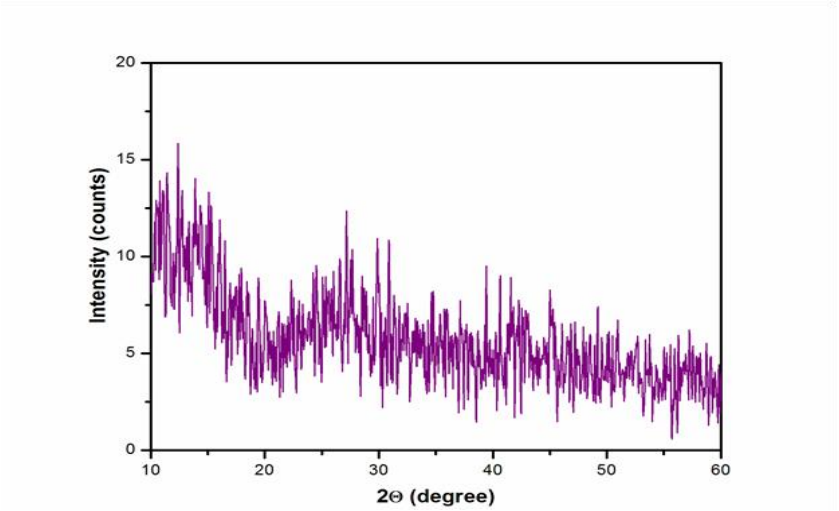

Fig .1 *XRD spectrum of lithium borate host glass matrix*

4. RAMAN SPECTRUM:

The structural characteristics of the lithium borate host glass were examined using **Raman spectroscopy**. The Raman spectrum was recorded in the spectral range of **300–2000 cm⁻¹**, as shown in **Figure 2.**

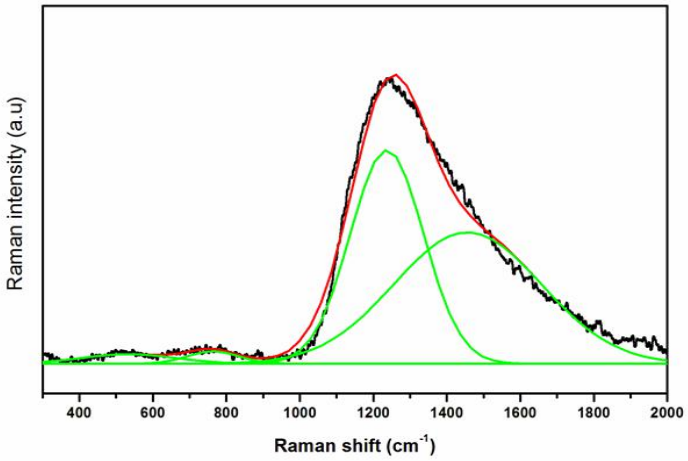

Fig. 2 *Raman spectrum of lithium borate host glass matrix*

To gain deeper insight into the specific **structural units** present in the glass matrix, the Raman spectrum was **deconvoluted using Gaussian peak fitting**. The fitting was performed based on the position, width, and number of observed bands, and yielded a good agreement with the original spectrum. As illustrated in **Fig.2**, the **black line** represents the experimental Raman spectrum, the **red line** corresponds to the overall Gaussian fit, and the **green lines** denote the individual deconvoluted peaks. The close overlap between the fitted curve and the experimental data confirms the **accuracy and reliability** of the fitting process, with minimal deviation. The **Raman band at ~492 cm⁻¹** is attributed to vibrations associated with **penta-, tetra-, and diborate rings**. The **peak around 755 cm⁻¹** arises from the **symmetric stretching vibrations** of structural units such as **di-triborates, triborates, tetraborates, pentaborates**, and various **six-membered ditriborate rings**. A band observed near **1230 cm⁻¹** corresponds to the **symmetric stretching of B–O– B bridges** and **terminal B–O vibrations** within **pyroborate units**, indicating the presence of diverse borate linkages in the glass network. Additionally, when the **oxide modifier content is below 50 mol%**, a shift near **1468 cm⁻¹** is typically associated with **asymmetric stretching modes of triangular borate groups** [8–12]. These findings further validate the complex and diverse nature of the borate network in the synthesized glass, contributing to its desirable optical characteristics.

5. OPTICAL ABSORPTION ANALYSIS:

The UV–VIS and NIR absorption spectra of the LB glass matrix doped with 0.5 mol% Dy_2O_3 are presented in Figures 3a and 3b, respectively.

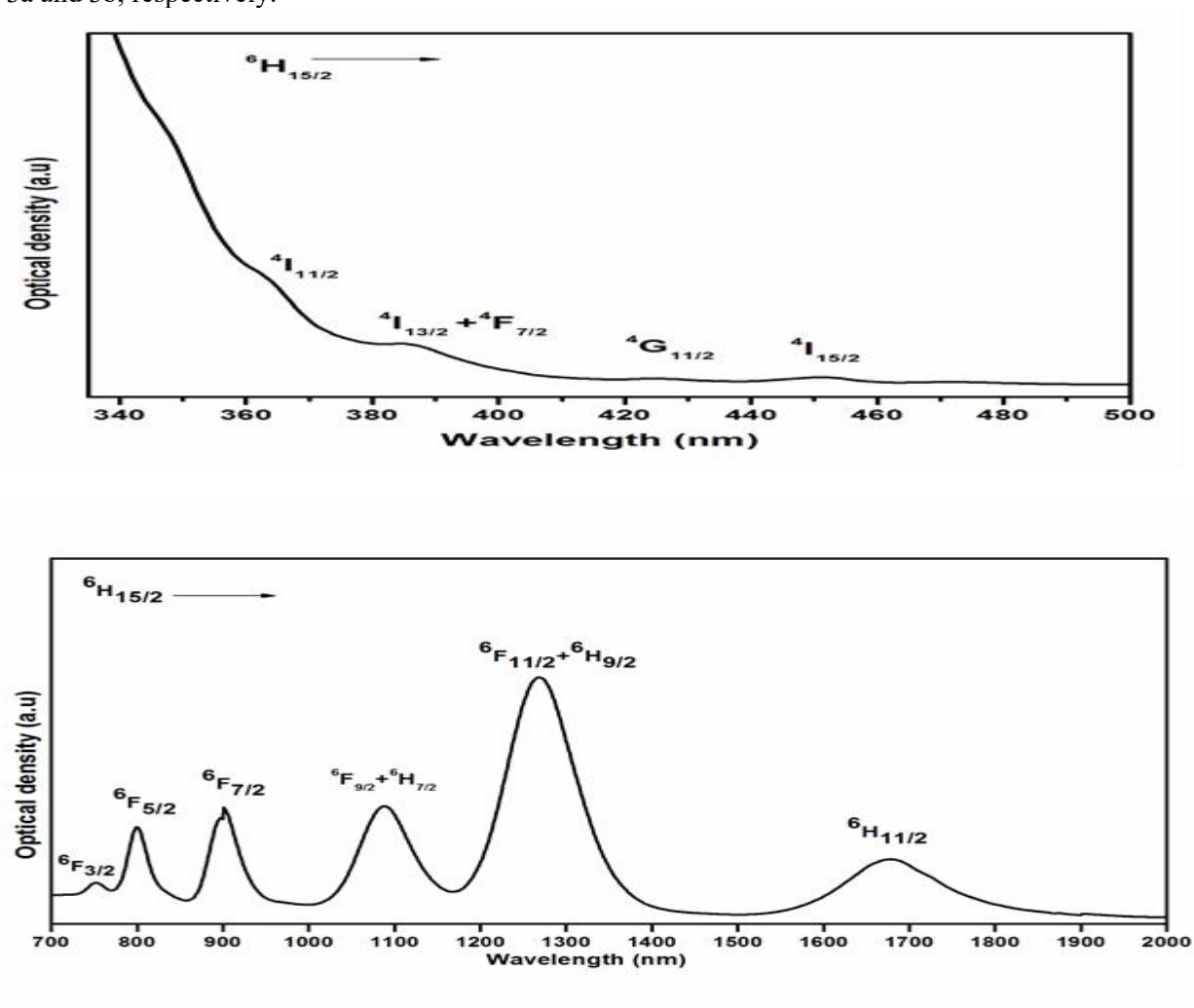

Fig. 3 (a) *UV-VIS* **(b)** *NIR absorption spectrum of 0.5 mol% of Dy3+ doped lithium borate glass matrix*

In the NIR region, the most intense absorption band—assigned to the $^6F_{11/2}+^6H_{9/2}$ transition—is centered at 7874 cm^{-1}. The observed transitions from the ground state $^6H_{15/2}$ to various ^6H and ^6F excited levels are spin-allowed ($\Delta S=0$). Furthermore, transitions confined within the ^6H manifold obey the orbital angular momentum selection rule ($\Delta L=0$), which contributes to their notably high intensity in the near-infrared. The spectral oscillator strengths—experimental (f_{exp}) and theoretical (f_{cal})—for the 0.5 mol% Dy_2O_3-doped LB glass matrix were determined, and the root-mean-square deviation (δ_{rms}) between them was calculated. The results are summarized in Table 1.

Table 1:
The oscillator strengths or spectral intensities ($\times 10^{-6}$) of 0.5 mol% Dy^{3+} doped for LB05Dy glass matrix

Transition $^6H_{15/2} \rightarrow$	f_{exp}	f_{cal}
$^4I_{13/2}+^4F_{7/2}$	4.18	3.94
$^4G_{11/2}$	0.24	0.14
$^4I_{15/2}$	0.73	0.82

$^4F_{9/2}$	0.26	0.25
$^6F_{3/2}$	0.41	0.32
$^6F_{5/2}$	2.44	1.92
$^6F_{7/2}$	3.27	3.08
$^6F_{9/2}+{}^6H_{7/2}$	4.16	4.01
$^6F_{11/2}+{}^6H_{9/2}$	11.11	11.17
$^6H_{11/2}$	2.07	2.27
	δ_{rms} $\pm 0.53\times10^{-6}$	

The experimental oscillator strengths (f_{exp}) for the observed absorption bands were determined using the expression provided in Ref. [13], whereas the theoretical oscillator strengths (f_{cal}) were computed via Judd–Ofelt (J–O) theory [14, 15]. Analysis of Table 1 reveals that among the various electronic transitions, the $^6H_{15/2}\rightarrow{}^6F_{11/2}+{}^6H_{9/2}$ transition exhibits the highest spectral intensity ($\sim 11.11\times10^{-6}$), indicating pronounced asymmetry and a distinctive coordination environment surrounding the Dy^{3+} ions. The Judd–Ofelt intensity parameters, Ω_λ ($\lambda = 2, 4, 6$), offer insight into the local structure and bonding at rare-earth ion sites. Notably, Ω_2 correlates with the asymmetry and covalency of the RE–ligand bond—a larger Ω_2 reflects stronger covalent character and lower site symmetry .In contrast, Ω_4 and Ω_6 are largely influenced by the host matrix's rigidity, viscosity, and bulk properties, and are less sensitive to the immediate surroundings of the RE ions. From the spectral intensities, the Ω_l values were derived using least-squares fitting of squared reduced matrix elements (per J–O theory), and the computed values are summarized in Table 2.

Table 2: A comparison of J–O intensity parameters (Ω_λ, $\times10^{-20}$ cm^2) of 0.5 mol% of Dy^{3+} - doped LB05 glass matrix and other different glasses

Glass	Ω_2	Ω_4	Ω_6	Order	Reference
LB05	9.30	3.07	2.41	$\Omega_2>\Omega_4>\Omega_6$	Present work
Tellurite	6.91	0.99	1.01	$\Omega_2>\Omega_6>\Omega_4$	[17]
Aluminofluoro - borophosphate	6.28	5.21	1.10	$\Omega_2>\Omega_4>\Omega_6$	[18]
Oxyfluorotellurite	2.32	0.64	4.64	$\Omega_2>\Omega_6>\Omega_4$	[19]
zinc–sodium–aluminosilicate	0.54	0.10	0.03	$\Omega_2>\Omega_4>\Omega_6$	[20]
LGBiBDy1.5	13.63	13.41	3.53	$\Omega_2>\Omega_4>\Omega_6$	[21]

From Table 2, the Judd–Ofelt parameter Ω_2 for the LB05Dy glass is determined to be 9.30×10^{-20} cm^2. This high Ω_2 value indicates stronger covalency compared to other glasses such as tellurite, aluminofluoro-borophosphate, oxyfluorotellurite, and zinc–sodium–aluminosilicate types. In contrast, it remains lower than that found in the $LGBiBDy_{1.5}$ glass. Moreover, the intensity trend across the Ω_l parameters for LB05Dy follows: $\Omega2>\Omega4>\Omega6$.

6. LUMINESCENCE SPECTRA:

The excitation spectrum of the 0.5 mol% Dy_2O_3-doped lithium borate glass matrix was measured over the 300–500 nm range, with emission monitored at 573 nm. The resulting spectrum is displayed in Figure 4.

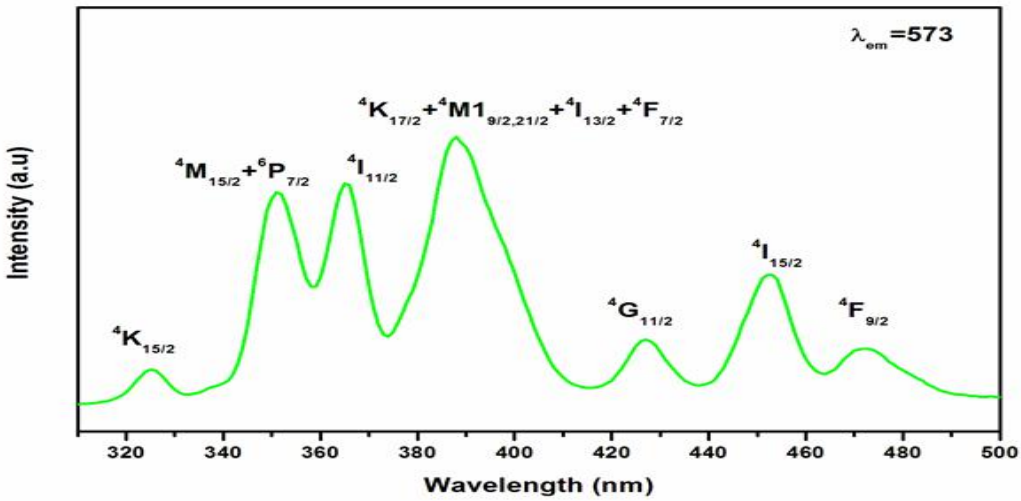

Fig .4 *Excitation spectrum of 0.5 mol% of Dy3+ doped lithium borate glass matrix*

The excitation spectrum comprises seven distinct, inhomogeneous peaks corresponding to transitions from the ground state level $^6H_{15/2}$ to the excited states located at 325 nm ($^4K_{15/2}$), 350 nm ($^4M_{15/2}$+ $^6P_{7/2}$), 364 nm ($^4I_{11/2}$), 388 nm ($^4K_{17/2}$+$^4M_{19/2,21/2}$+$^4I_{13/2}$+$^4F_{7/2}$), 427 nm ($^4G_{11/2}$), 452 nm ($^4I_{15/2}$) and 471 nm ($^4F_{9/2}$). Among these, the 388 nm peak exhibits notably higher intensity and was thus selected for subsequent luminescence measurements.

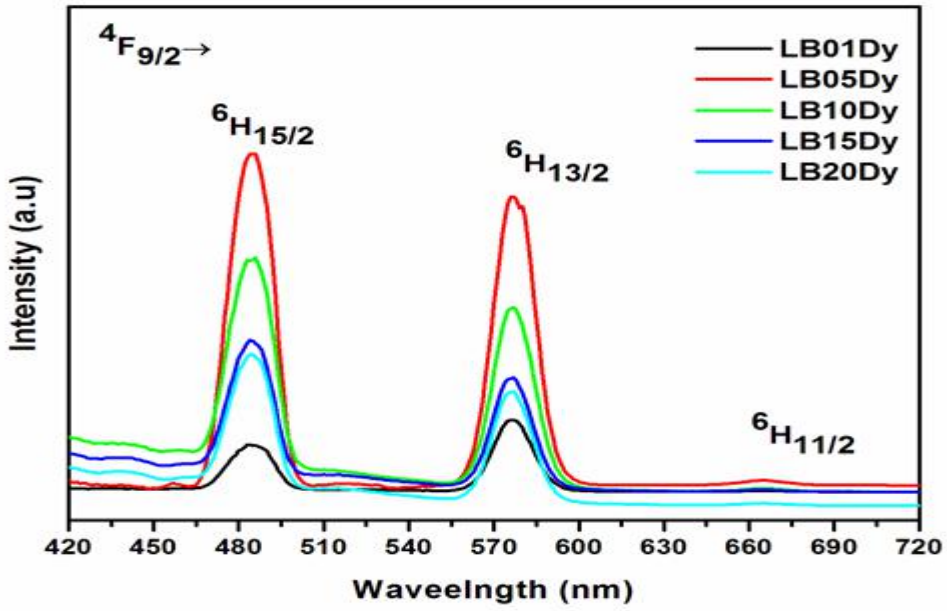

Fig.5 *Emission spectra of Dy3+ doped lithium borate glass matrix with different concentrations*

7. VISIBLE FLUORESCENCE SPECTRA:

Figure 5 displays the visible fluorescence spectra of lithium borate glasses doped with varying concentrations of Dy_2O_3, recorded at an excitation wavelength of 388 nm. Upon excitation, Dy^{3+} ions are promoted from the ground state ($_6H_{15/2}$) to higher energy levels such as $^4I_{13/2}$+$^4F_{7/2}$. These excited ions then relax non-radiatively to the metastable $^4F_{9/2}$ level, owing to the small energy gap between adjacent states. Because the energy gap between $^4F_{9/2}$ and the lower level $^6F_{3/2}$ is relatively large, non-radiative decay is suppressed, and radiative emissions dominate. The emission spectrum features three prominent transitions from the $^4F_{9/2}$ level to the ^6H_J (J = 15/2, 13/2, 11/2) levels, corresponding to blue (~484 nm), yellow (~573 nm), and red (~663 nm) emissions, respectively. Among these, the yellow emission

($^4F_{9/2}\rightarrow{}^6H_{13/2}$) at 573 nm shows the highest intensity, while the red emission at 663 nm is the weakest. The blue emission at 484 nm exhibits moderate intensity [18, 19]. The blue emission transition ($^4F_{9/2}\rightarrow{}^6H_{15/2}$)is a magnetic dipole (MD) transition and is relatively insensitive to the local crystal field. In contrast, the yellow emission ($^4F_{9/2}\rightarrow{}^6H_{13/2}$ is an electric dipole (ED) transition ($\Delta L = 2$, $\Delta J = 2$), classified as a hypersensitive transition. Its intensity strongly reflects the asymmetry and covalency of the local environment around the Dy^{3+} ions [20]. The intensity ratio of the electric dipole to magnetic dipole transitions (ED/MD), often referred to as the yellow-to-blue (Y/B) ratio, serves as an indicator of the asymmetry around Dy^{3+} ions [32]. In this study, Y/B ratios were found to be 1.52, 0.88, 0.82, 0.78, and 0.72 for LB01Dy, LB05Dy, LB10Dy, LB15Dy, and LB20Dy glasses, respectively. A higher Y/B ratio implies a greater degree of covalency and asymmetry. Therefore, LB01Dy exhibits the highest local asymmetry and covalency, while LB20Dy shows the lowest. As Dy_2O_3 concentration increases, the Y/B ratio decreases, indicating a reduction in covalent character around the Dy^{3+} ions.

Notably, emission intensity increases with Dy_2O_3 concentration up to 0.5 mol%, peaking in the LB05Dy sample. Beyond this point, a decline in intensity is observed, particularly in the LB20Dy glass. This decrease is attributed to concentration quenching, which becomes significant at Dy^{3+} concentrations above 0.5 mol%. As the dopant concentration rises from 0.5 to 2.0 mol%, non-radiative energy transfer mechanisms such as cross-relaxation and resonant energy transfer become more active, thereby reducing fluorescence efficiency. The luminescence properties such as peak emission wavelengths (λ_P), effective bandwidths ($\Delta\lambda_{eff}$), branching ratios (β) (experimental), transition probability (A_R), peak emission cross-sections (σ_e) and optical gain ($\sigma_e\times\tau_{exp}$) for the three emission transitions $^4F_{9/2}\rightarrow{}^6H_J$ (J=15/2, 13/2, and 11/2) are calculated for LB05Dy glass matrix and are presented in Table 3.

Table 3: Luminescence parameters of 0.5 mol% Dy^{3+} doped LBDy05 glass matrix.

Parameters	$^4F_{9/2} \rightarrow {}^6H_{15/2}$	$^4F_{9/2} \rightarrow {}^6H_{13/2}$	$^4F_{9/2} \rightarrow {}^6H_{11/2}$
λ_p (nm)	484	573	665
$\Delta\lambda_{eff}$ (nm)	19	17	20
A_R (s^{-1})	202	871	89
β_{exp}	0.49	0.46	0.05
τ_{exp} (ms)	0.79	0.79	0.79
σ_e ($\times10^{-22}$ cm^2)	6.17	18.95	4.32
$\sigma_e\times\tau_{exp}$ ($\times10^{-25}$ cm^2-sec)	4.87	14.97	3.41

The equations employed were sourced from Ref. [17] and used to derive all the luminescence parameters. Experimental branching ratios (β_exp) were obtained by integrating each specific emission peak. The branching ratios (β), peak emission cross-sections (σ_e), and optical gain ($\sigma_e\times\tau$_exp) are key metrics for assessing the lasing potential of the transitions.

Based on Table 3:

- The branching ratios for the $^4F_{9/2}\rightarrow{}^6H_{13/2}$ and $^4F_{9/2}\rightarrow{}^6H_{15/2}$transitions are significantly higher than that for $^4F_{9/2}\rightarrow{}^6H_{11/2}$
- The radiative transition probability ARA_RAR for the yellow transition ($^4F_{9/2}\rightarrow{}^6H_{13/2}$) is highest (871 s^{-1}), compared to 202 s^{-1} for the blue transition and 89 s^{-1} for the red.
- A high σ_e (18.95×10^{-22} cm^2) for the $^4F_{9/2}\rightarrow{}^6H_{13/2}$ transition suggests strong laser amplification potential, as larger emission cross-sections correspond to lower lasing thresholds and higher gain—a principle well noted in Dy^{3+}-doped laser materials.
- Optical gain ($\sigma_e\times\tau$_exp) follows the same pattern, peaking at 14.97×10^{-25} $cm^2\cdot s$ for the yellow transition, compared to 4.87×10^{-25} for blue and 3.41×10^{-25} for red.

Altogether, the elevated ARA_RAR, σ_e, and optical gain centered on the 574 nm yellow emission indicate that the $^4F_{9/2}\rightarrow{}^6H_{13/2}$ transition in the 0.5 mol% Dy_2O_3-doped LB glass (LB05Dy) is the most promising candidate for yellow-lasing applications.

8. DECAY CURVE ANALYSIS:

Fluorescence decay profiles of the 4F9/2 emission level were recorded at room temperature for lithium borate glasses doped with varying concentrations of Dy_2O_3 (0.1, 0.5, 1.0, 1.5, and 2.0 mol%), using excitation at 388 nm and monitoring emission at 573 nm (see Fig. 6).

- **Single-exponential decay at low concentrations**: For LB01Dy (0.1 mol%) and LB05Dy (0.5 mol%) samples, the decay is well-described by a single exponential function, indicating negligible Dy^{3+}–Dy^{3+} interactions.
- **Non-exponential decay at higher concentrations**: In samples with Dy^{3+} concentrations above 0.5 mol% (LB10Dy, LB15Dy, LB20Dy), the decay curves deviate from single-exponential behavior and are best fitted using the Inokuti–Hirayama model—with s=6s = 6s=6, confirming that dipole–dipole interactions dominate the energy transfer mechanism.

As Dy^{3+} concentration increases, the decay profiles become increasingly non-exponential due to enhanced donor-to-acceptor energy transfer (cross-relaxation) between excited 4F9/2^{4}F_{9/2}4F9/2 ions and ground-state 6H15/2 ions. This interaction results in shorter experimental lifetimes (τ_{exp}):

- LB01Dy: 0.80 ms
- LB05Dy: 0.79 ms
- LB10Dy: 0.65 ms
- LB15Dy: 0.49 ms
- LB20Dy: 0.30 ms

The systematic decrease in τ_{exp} with increasing Dy^{3+} concentration reflects the growing influence of non-radiative processes driven by cross-relaxation and resonant energy transfer. These findings align with observations in other Dy^{3+}-doped glass systems, where decay evolves from single to non-exponential as dopant concentration increases—with dipole-dipole coupling (s = 6) identified as the dominant mechanism

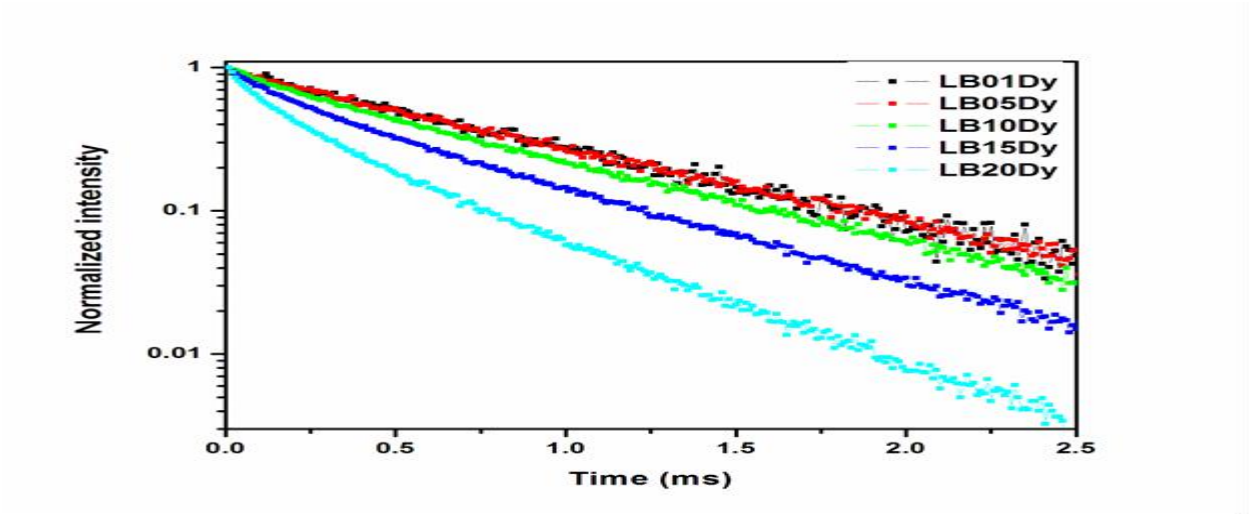

Fig.6 *Decay profiles of Dy3+ doped lithium borate glass matrix with different Concentrations*

9. CONCLUSIONS:

- **Glass Preparation & Structural Characterization**
  Lithium borate glasses doped with Dy^{3+} (0.1–2 mol% Dy_2O_3) — composition: (60−x)(60-x)(60−x) B_2O_3 + 20 LiF + 10 MgF_2 + 10 ZnO + x Dy_2O_3 — were successfully synthesized via melt-quenching. XRD confirmed their amorphous nature, while Raman spectra revealed various borate ring structures (di-, tri-, tetra-, penta-borates).
- **Optical Absorption & Judd–Ofelt Analysis** Judd–Ofelt parameters for the 0.5 mol% Dy^{3+} glass (LB05Dy) were determined as $\Omega_2 = 9.30 \times 10^{-20}$ cm², $\Omega_4 = 3.07 \times 10^{-20}$ cm², and $\Omega_6 = 2.41 \times 10^{-20}$ cm², following the trend $\Omega_2 > \Omega_4 > \Omega_6$. These values reflect significant site asymmetry and covalent Dy^{3+}–ligand bonding.
- **Radiative & Emission Properties** Using the Judd–Ofelt framework, radiative transition probabilities, experimental branching ratios, emission cross-sections, and optical gain were computed for the 4F9/2→6HJ^{4}F_{9/2} \to {}^{6}H_J4F9/2→6HJ transitions.

- **Luminescence & Concentration Effects** Photoluminescence intensity increased with Dy^{3+} loading up to 0.5 mol%, and then diminished due to concentration quenching beyond this level. This behavior is attributed to efficient non-radiative energy transfer mechanisms (cross-relaxation and resonant interactions).
- **Optimized Yellow Emission** For the LB05Dy glass, the 4F9/2→6H13/2^{4}F_{9/2} \to {}^{6}H_{13/2}4F9/2→6H13/2 yellow emission at 573 nm exhibited superior radiative parameters (highest ARA_RAR, σe\sigma_eσe, and σe×τexp\sigma_e \times \tau_{\rm exp}σe×τexp), confirming its exceptional suitability as a yellow lasing medium.
- **Decay Dynamics** Lifetimes (τexp\tau_{\rm exp}τexp) decreased systematically with increasing Dy^{3+} concentration (from 0.80 ms at 0.1 mol% to 0.30 ms at 2.0 mol%), indicating enhanced non-radiative decay due to Dy^{3+}–Dy^{3+} interactions and energy transfer. The transition from single-exponential to non-exponential decay further corroborates energy transfer dynamics among Dy^{3+} ions.
- **Overall Assessment** Among the series, LB05Dy (0.5 mol% Dy_2O_3) demonstrates the most balanced and efficient luminescent behavior — combining strong yellow emission, high optical gain, and suppressed concentration quenching. This positions LB05Dy as a promising candidate for yellow laser and visible photonic applications, in agreement with similar Dy^{3+}-doped lithium borate glass systems in recent literature

REFERENCES:

1. Lu, Y.; Yu, H. *J. Mater. Sci.: Mater. Electron.* **25**, 1013–1016 (2014).
2. Bhushana Reddy, M.; Sailaja, S.; Nageswara Raju, C.; Sudhakar Reddy, B. *J. Opt.* **43**, 101–107 (2014).
3. Venkatramu, V.; Babu, P.; Jayasankar, C. K. *Spectrochim. Acta A* **63**, 276–281 (2006).
4. Chemingui, S.; Ferhi, M.; Horchani-Naifer, K.; Férid, M. *J. Lumin.* **166**, 82–87 (2015).
5. Hashim, S.; Mhareb, M. H. A.; Ghoshal, S. K.; Alajerami, Y. S. M.; Bradley, D. A.; Saripan, M. I.; Tamchek, N.; Alzimami, K. *Radiat. Phys. Chem.* **116**, 138–141 (2015).
6. Meza-Rocha, A. N.; Speghini, A.; Bettinelli, M.; Caldiño, U. *J. Lumin.* **176**, 235–239 (2016).
7. Mhareb, M. H. A.; Hashim, S.; Ghoshal, S. K.; Alajerami, Y. S. M.; Bqoor, M. J.; Hamdan, A. I.; Saleh, M. A.; Abdul Karim, M. K. B. *J. Lumin.* **177**, 366–372 (2016).
8. Dwivedi, B. P.; Khanna, B. N. *J. Phys. Chem. Solids* **56**, 39–49 (1995).
9. Osipov, A. A.; Osipova, L. M. *J. Phys. Chem. Solids* **74**, 971–978 (2013).
10. Dias, J. D. M.; Melo, G. H. A.; Lodi, T. A.; Carvalho, J. O.; Façanha Filho, P. F.; Barboza, M. J.; Steimacher, A.; Pedrochi, F. *J. Rare Earths* **34**, 521 (2016).
11. Subhadra, M.; Kistaiah, P. *Vib. Spectrosc.* **62**, 23–27 (2012).
12. Osipov, A. A.; Osipova, L. M. *Physica B* **405**, 4718–4732 (2010).
13. Kuhn, S.; Herrmann, A.; Rüssel, C. *J. Lumin.* **157**, 390–397 (2015).
14. Judd, B. R. *Phys. Rev.* **127**, 750 (1962).
15. Ofelt, G. S. *J. Chem. Phys.* **37**, 511 (1962).
16. Ravi, O.; Madhukar Reddy, C.; Sudhakar Reddy, B.; Deva Prasad Raju, B. *Opt. Commun.* **312**, 263–268 (2014).
17. Venkataiah, G.; Jayasankar, C. K. *J. Mol. Struct.* **1084**, 182–189 (2015).
18. Vijayakumar, M.; Marimuthu, K. *J. Lumin.* **178**, 414–424 (2016).
19. Klimesz, B.; Romanowski, W. R.; Lisiecki, R. *Opt. Mater.* **42**, 538–543 (2015).
20. Caldiño, U.; Lira, A.; Meza-Rocha, A. N.; Pasquini, E.; Pelli, S.; Speghini, A.; Bettinelli, M.; Righini, G. C. *J. Lumin.* **167**, 327–332 (2015).
21. Zaman, F.; Kaewkhao, J.; Srisittipokakun, N.; Wantana, N.; Kim, H. J.; Rooh, G. *Opt. Mater.* **55**, 136–144 (2016).